This is the Pre-Published Version.

The following publication Zhang, Y.-H., Huang, X.-H., Wong, W.-L., Luo, J.-R., Guo, X.-C., Liu, W., Hou, J., She, M.-T., Jiang, W.-H., Sun, N., & Lu, Y.-J. (2023). A red fluorescent small-molecule for visualization of higher-order cyclic dimeric guanosine monophosphate (c-di-GMP) structure in live bacterial cells and real-time monitoring of biofilm formation on biotic and abiotic surfaces. Sensors and Actuators B: Chemical, 376, 132992 is available at https://dx.doi.org/10.1016/j.snb.2022.132992.

POAA red fluorescent small-molecule for visualization of higher-order cyclic dimeric guanosine monophosphate (c-di-GMP) structure in live bacterial cells and real-time monitoring of biofilm formation on biotic and abiotic surfaces

Yi-Han Zhang [a], Xuan-He Huang [a], Wing-Leung Wong [b,*], Jun-Ren Luo [a], Xiao-Chun Guo [a], Wenjie Liu [d,e], Jinqiang Hou [d,e], Meng-Ting She [a], Wen-Hao Jiang [a], Ning Sun [c,*] and Yu-Jing Lu [a,*]

[a] School of Biomedical and Pharmaceutical Sciences, Guangdong University of Technology, Guangzhou 510006, P. R. China.

[b] State Key Laboratory of Chemical Biology and Drug Discovery, Department of Applied Biology and Chemical Technology, The Hong Kong Polytechnic University, Hung Hom, Kowloon, Hong Kong SAR, China.

[c] Guangzhou First People's Hospital, School of Medicine, South China University of Technology, Guangzhou 510180, P. R. China.

[d] Department of Chemistry, Lakehead University, 955 Oliver Road, Thunder Bay, Ontario P7B 5E1, Canada.

[e] Thunder Bay Regional Health Research Institute, 980 Oliver Road, Thunder Bay, Ontario P7B 6V4, Canada.

* Corresponding author

E-mail (Wing-Leung Wong): wing.leung.wong@polyu.edu.hk

E-mail (Ning Sun): ning.sun@connect.polyu.hk

E-mail (Yu-Jing Lu): luyj@gdut.edu.cn

© 2022. This manuscript version is made available under the CC-BY-NC-ND 4.0 license http://creativecommons.org/licenses/by-nc-nd/4.0/.

Abstract

Cyclic dimeric guanosine monophosphate (c-di-GMP) is an important second messenger in bacteria. It regulates a wide range of bacterial functions and behaviors including biofilm formation that causes chronic infections and antibiotic resistance. C-di-GMP being as a signal transducer in bacteria is known to exist in monomer and dimer form. Recent studies also discover that c-di-GMP can form higher-order oligomers, such as tetramer and octamer, which may have physiological roles in bacterial cells. Moreover, the tetrameric c-di-GMP structure was reported to link two subunits of a transcription factor (BldD), which controls the progression of multicellular differentiation in sporulating actinomycete bacteria and then mediates the dimerization process. Current understanding on higher-order oligomers of c-di-GMP is relatively limited compared to its monomer or dimer structure. To probe and visualize the higher-order structure of c-di-GMP and its associated biofunctions in live bacterial cells with fluorescence techniques for mechanistic study and cellular investigation is important. Nonetheless, the sensitive and selective fluorescent probe with a rapid signal response for higher-order oligomers of c-di-GMP is currently lacking. In the present study, a series of fluorescent probes that preferentially interacted with tetrameric c-di-GMP and generated red fluorescence signal promptly were synthesized and investigated. The interaction mechanism was studied with ^{1}H NMR and molecular docking. In addition, the ligand was demonstrated as an excellent molecular fluorescent probe for bioimaging of tetrameric c-di-GMP structure and monitoring of biofilm formation on both biotic and abiotic surfaces with pathogenic bacteria including *Pseudomonas aeruginosa* PAO1 and *Bacillus subtilis* 168.

Keywords: Red fluorescent biosensor; Biotic and abiotic surfaces; Visualization of biofilm formation; Real-time monitoring; C-di-GMP tetramer; Medical and implant devices

1. Introduction

Bis-(3′-5′)-cyclic dimeric guanosine monophosphate (c-di-GMP) discovered in 1987 has been known as a very important bacterial nucleotide-based second messenger [1] and exists universally in bacteria [2, 3]. This small biomolecule not only regulates bacterial life-style transitions from motile to sessile phase, but also plays crucial roles in many bacterial functions such as cell division, exopolysaccharide synthesis, virulence and biofilm formation [4-6]. It is generally believed that the disruption of c-di-GMP homeostasis in bacteria may influence bacterial growth and survival [7, 8]. Due to the high importance of c-di-GMP to many bacterial functions, the detection, visualization, and monitoring of intracellular c-di-GMP for the study of its biological functions are significant. The investigation of intracellular c-di-GMP may also provide vital information for the discovery of effective compounds to reduce bacterial virulence, inhibit biofilm formation and address the antimicrobial resistance [9-11].

Despite c-di-GMP analysis mostly relays on LC-MS techniques, the fluorescence-based method that can be used for real-time detection, imaging and monitoring of c-di-GMP within bacterial cells is more attractive and useful for mechanistic studies in live bacterial cells [12]. Some recent examples developed include the fluorescent protein or luciferase fused reporter sensors [13-16], riboswitch-based biosensors [17-22], split-protein reporters [23, 24], FRET-based biosensors [25-30], chemiluminescent biosensors [31] and bioluminescence resonance energy transfer-based biosensors [32]. All these biosensing systems are targeting monomeric c-di-GMP; however, structural analysis of c-di-GMP showed that, in addition to the monomeric form of c-di-GMP, a stable dimer with stacked self-intercalated guanine residues was also found [5, 33]. Interestingly, both forms were found in crystal structures of c-di-GMP-binding and c-di-GMP-metabolizing proteins [34-41]. Furthermore, c-di-GMP was found able to form stable higher-order oligomers such

as tetramers and octamers [33]. At present, whether these c-di-GMP oligomers taking physiological roles in bacterial cells is still unclear.

Molecular biosensors developed based on small organic molecules for bio-recognition and sensing of c-di-GMP are not commonly found in literature, particularly the biosensor targeting higher-order structures of c-di-GMP. It was reported that c-di-GMP was able to form tetramolecular and octamolecular complexes *in vitro* upon c-di-GMP molecules interacting with monovalent cations [42] such as K^+ ion and some small-sized probes including thiazole orange (**TO**) [43], acriflavine [44], diminazene aceturate [45], **A18** [46], **5h** [47]. In addition, **CDy11** [48] was found targeting bacterial amyloid (**Figure 1**). Moreover, recent studies have proposed an interesting strategy of inducing the formation of dysfunctional higher-order c-di-GMP oligomers [44, 47]. This approach may possibly interrupt the monomeric c-di-GMP signal pathway and thus interfere with its normal bacterial functions in bacterial growth and survival.

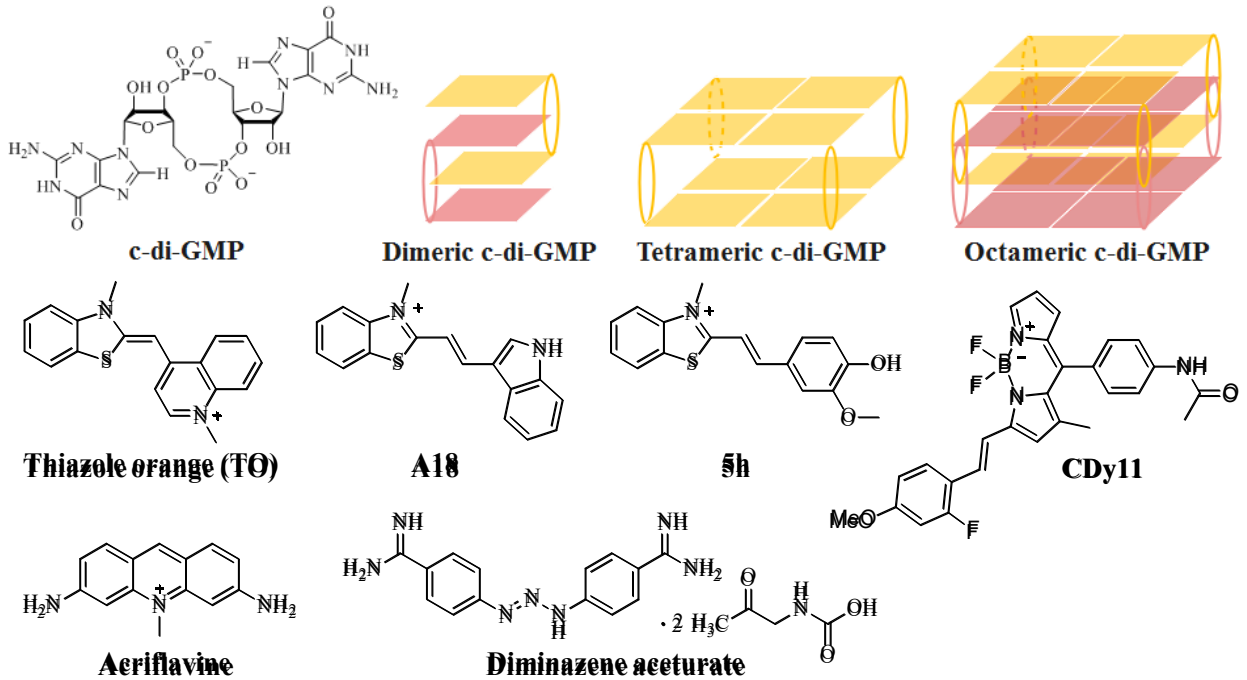

Figure 1. The structure of monomeric c-di-GMP and its proposed structures of dimeric, tetrameric and octameric form, and the recently reported ligands capable of interacting with bacterial c-di-GMP or amyloid.

To probe and visualize the formation of higher-order oligomers of c-di-GMP, such as tetramer and octamer, in live bacterial cells with fluorescence techniques is important for mechanistic study and cellular investigations. Sensitive and selective fluorescent probes can provide useful chemical tools for exploring the unknown physiological roles of these special structures in live bacterial cells with confocal microscopes. A recent report disclosed that c-di-GMP was able to assemble into a tetramer that mediates the dimerization of an effector protein (the transcription factor, BldD), which controls the progression of multicellular differentiation in sporulating actinomycete bacteria [49]. More importantly, the study *via* structural and biochemical analyses revealed that the second messenger c-di-GMP activated BldD DNA binding by driving a unique form of dimerization. Interestingly, the dimerization was mediated by a tetrameric form of c-di-GMP but not the monomer and dimer. However, the highly selective and sensitive fluorescent tool for recognition and imaging of cellular tetrameric c-di-GMP structure is currently lacking [12]. In the present study, we synthesized a series of red fluorescent probes that was able to interact with the higher-order tetrameric c-di-GMP structure selectively. The specific interaction rendered the instant generation of intensive and red fluorescence signal both *in vitro* and *in cellulo*. The molecular probe is small-sized, fast response, highly sensitive and selective toward the tetrameric c-di-GMP structure, and highly stable against photo-bleaching, and generally exhibits low toxicity toward human kidney and epithelial cells. Our mechanistic study with NMR spectroscopy also showed that the probe was able to induce the monomeric c-di-GMP molecule to form a stable tetramer and followed by producing fluorescence signal. In addition, molecular docking study illustrated that the probe interacted with the tetrameric c-di-GMP structure *via* the π-π stacking mode with the guanine residue and hydrogen bond interaction with the amide group of the guanine residue.

2. Experimental Section

All chemicals and reagents were purchased from commercial in AR grade and were used without further purifications. C-di-GMP and GMP were purchased from Sigma-Innochem. Deoxy-ribonucleoside triphosphates including dATP, dGTP, dCTP, and dTTP were purchased from New England Biolab. Ribonucleoside triphosphates including rGTP, rATP, rCTP, and rUTP were purchased from New England Biolab. cGMP was purchased from GLPBIO. Bruker Avance III 300 MHz Superconducting Fourier Nuclear Magnetic Resonance Spectrometer was used to record ^{1}H and ^{13}C NMR in deuterated solvent (DMSO-*d6*) at 24 °C using TMS as the reference. High-resolution mass spectrometry (HRMS) was obtained by Aglient 7250 TOF. High performance liquid chromatography (HPLC) analysis was performed with SHIMADZU LC-16 system using Diamonsil C18 column (250 × 4.6 mm, 5 μm) at UV 225 nm detection for analyzing the purity of the compounds. All compounds synthesized were characterized with ^{1}H NMR, ^{13}C NMR, HRMS and HPLC before using in assays. Scanning electron microscopy analyses for the probes were conducted with a TESCAN MIRA LMS scanning electron microscope and an Apreo 2 SEM scanning electron microscope (Thermo Fisher). The detailed synthesis and characterization of the fluorescent probes **1-3** and methods for *in vitro* assays were given in Supporting Information.

3. Results and Discussion

3.1 Synthesis of probes and the study their interaction specificity with c-di-GMP

The red fluorescent probes targeting c-di-GMP tetramer were synthesized *via* a three-step preparation as shown in **Scheme 1** by adopting the reported procedures [50]. The pure compounds were obtained by recrystallization in ethanol under room temperature conditions. The characterizations performed with NMR, HRMS and SEM (**Figure S1-S4**) were found consistent

with literature [50]. We then used ultraviolet-visible absorption analysis to study the molecular interaction characteristics between the probe and c-di-GMP. The probe was designed to be flexible and the free rotation of the molecule in solution resulted in almost no emission. Nonetheless, when the probe interacts with its binding target, c-di-GMP, the freedom of molecular rotations is restricted and then the intensive emission signal corresponding to the interaction is generated [51]. The intensive emission signals were observed instantly upon mixing the probe with c-di-GMP under room temperature conditions and the maximum intensity was achieved in 5 min (**Figure S5A**). As shown in **Figure 2A**, when increasing c-di-GMP concentration in the titration, the intensity of absorption bands of the probe in the range from 325 to 450 nm was generally decreased, while a new peak at about 470 nm was clearly observed. Interestingly, for probe **3**, an isosbestic point appears at approximately 448 nm, which may indicate the *in-situ* formation of a unique and stable c-di-GMP-**3** adduct and there is no intermediate formed during the titration. In the fluorescence titration, the probes in their free rotation status showed very weak background emission signal in buffer solution without adding c-di-GMP substrates. However, after the addition of c-di-GMP, as shown in **Figure 2B**, the red fluorescence signal (λ_{em} = 636 nm) was generated markedly upon excited at 422 nm. The emission intensity was increased with respect to the amount of c-di-GMP added in the titration experiments. A large Stokes shift (194 nm) and good fluorescence quantum yield (Φf: 0.1-0.18) were observed. The fluorescence lifetime measured was found in the range of 1.67–1.83 ns (**Table 1** and **Figure S6-S7**).

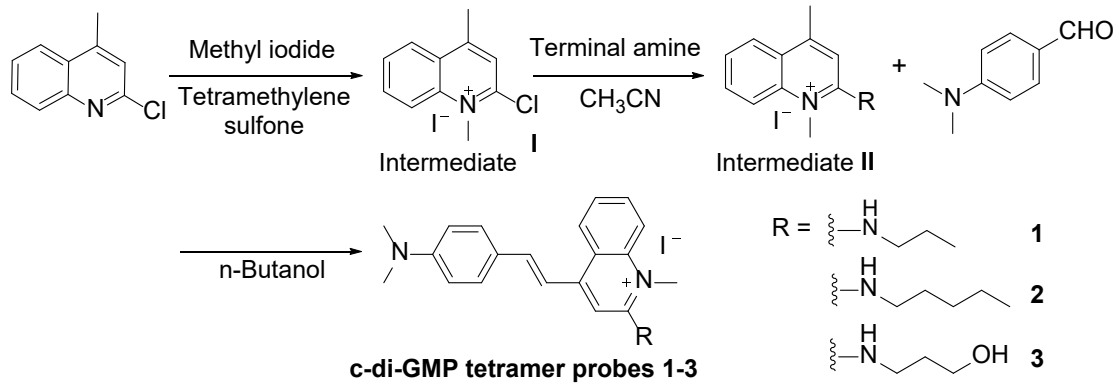

Scheme 1. The synthetic route to fluorescent probes **1**-**3**.

Table 1. The spectroscopic properties of the fluorescent probes.

Probe [a]	λ_{ex} (nm)	λ_{em} (nm)	Stokes shift (nm)	Φf [b]	Fluorescence lifetime (ns)
1	442	636	194	0.10 (0.05) [c]	1.67 (1.55) [c]
2	442	636	194	0.12 (0.04) [c]	1.75 (1.38) [c]
3	442	636	194	0.18 (0.03) [c]	1.83 (1.27) [c]

[a] The concentration of the probes used was 5.0 μM and the final concentration of c-di-GMP was 10.0 μM. The buffer used for assays was Tris-HCl (10 mM, pH 7.5) containing 60 mM KCl.

[b] Absolute fluorescence quantum yield of each fluorescent probe combined with c-di-GMP (Φf_A) and the absolute fluorescence quantum yield of fluorescein sodium combined with c-di-GMP (Φf_B = 35.12) was measured. Relative fluorescence quantum yield calculated by $\Phi f = \Phi f_A/\Phi f_B$.

[c] Numbers shown in parenthesis were obtained under the conditions without c-di-GMP.

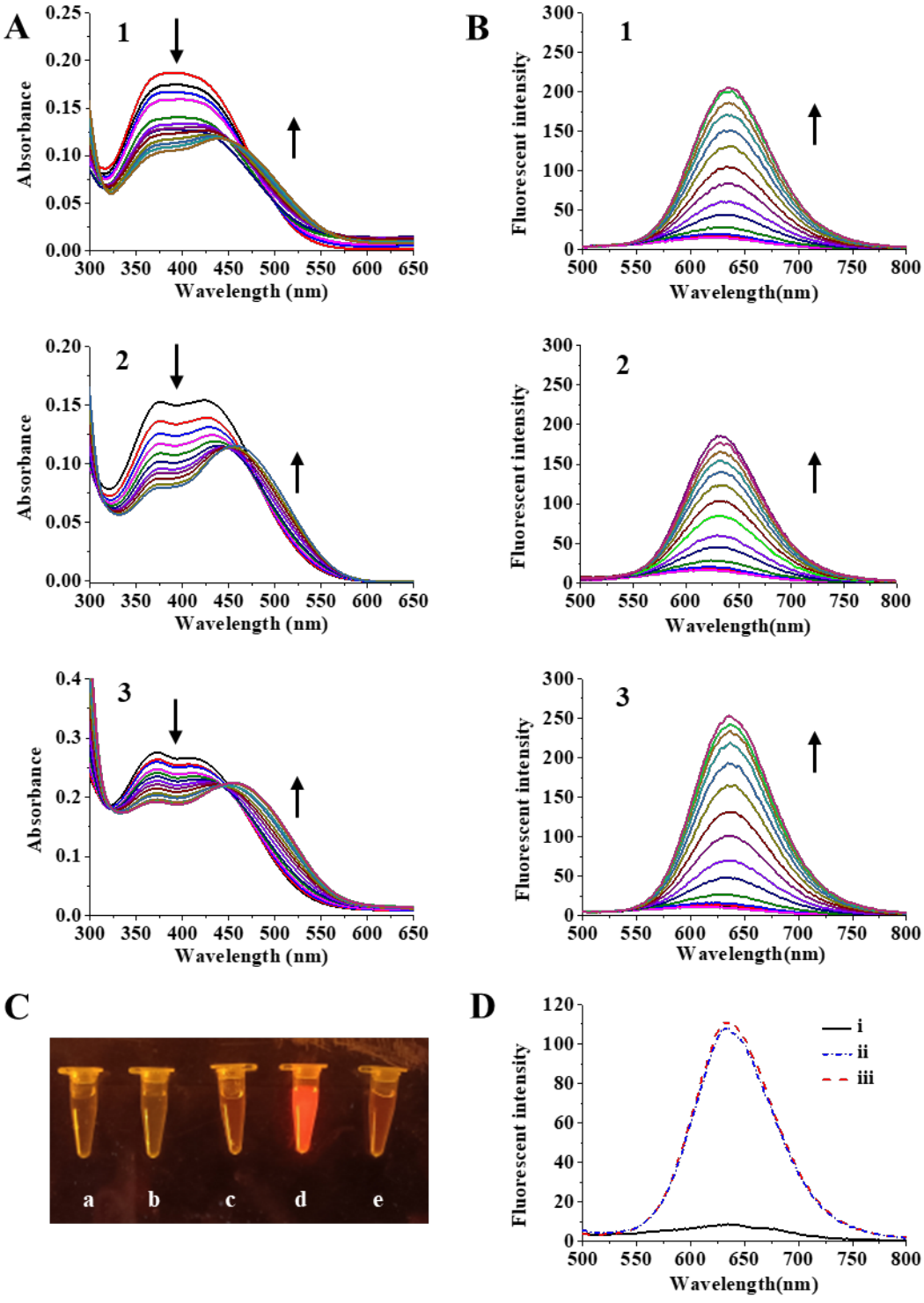

Figure 2. (A) UV-vis titration of **1-3** (15 μM) with c-di-GMP (0-50 μM). (B) Fluorescence spectroscopy of **1-3** (5 μM) with c-di-GMP (0-42 μM) in buffer solution. (C) Naked-eye

visualization of **3** (5 μM) complexed with c-di-GMP (10 μM) in buffer solution under a portable blue LED illuminator (470 nm, 30 W); A commercial dye **TO** (5 μM) was tested for comparison. (D) Selectivity and competition study of **3** (5 μM) with c-di-GMP (10 μM) and other nucleotides including GMP, cGMP, deoxy-ribonucleoside triphosphates (dATP, dGTP, dCTP and dTTP) and ribonucleoside triphosphates (rGTP, rATP, rCTP and rUTP); the concentration of each nucleotide was 10 μM; λ_{ex}= 442 nm. Buffer solution used for titrations and competition assays was Tris-HCl (10 mM, pH 7.5) containing 60 mM KCl.

The instant and intensive red fluorescence signal for the interaction of **3** and c-di-GMP upon mixing in buffer solution was readily observable by naked-eye under a portable blue LED illuminator (excitation at 470 nm) (**Figure 2C**). In addition, other analogue nucleotides including GMP, cGMP, deoxy-ribonucleoside triphosphates (dATP, dGTP, dCTP and dTTP) and ribonucleoside triphosphates (rGTP, rATP, rCTP and rUTP) examined were not able to induce fluorescence signal. The results indicate that probe **3** is specific to c-di-GMP. A commercial dye, thiazole orange (**TO**), reported capable of interacting with c-di-GMP [43], was also tested in the c-di-GMP-**TO** interaction study under the same conditions for comparison because its molecular structure is similar to **3**. However, **TO** could only give yellow emission signal with much weaker intensity compared with that of **3**. Taken together, the results suggest that **3** possesses excellent target-specificity and signal response toward c-di-GMP.

To demonstrate further the selectivity of **3** toward c-di-GMP, competition assays with a panel of analogue nucleotides including GMP, cGMP, dATP, dGTP, dCTP, dTTP, rGTP, rATP, rCTP and rUTP was performed in buffer solution. From **Figure 2D**, the fluorescence signal was markedly induced upon c-di-GMP interacting with **3**. Then, the addition of all these 10 analogue nucleotides

(at 10 μM each) together to compete with c-di-GMP (10 μM) did not show significant reduction of the fluorescence signal. This may imply that the binding affinity of **3** toward c-di-GMP is much stronger than that of the analogue nucleotides in solution. We thus speculate that **3** may interact with a higher-order structure of c-di-GMP such as tetramer, but not the monomeric form [49].

3.2 Determination of sensitivity (LOD), binding affinity (K_D) and binding stoichiometry of the probe with c-di-GMP

We analyzed the sensitivity of probes in determination of the c-di-GMP in buffer solution with fluorescence technique. In the fluorescence titration experiments, as shown in **Figure 3A**, the fluorescence intensity of probes examined was found increased with the increase of c-di-GMP concentration and a linear range for c-di-GMP detection was found in the range of 0.285 – 20.0 μM. An excellent linear relationship with respect to the fluorescence signal enhancement of c-di-GMP-**3** interaction was established as shown in **Figure 3B**. The limit of detection (LOD) and equilibrium binding constants (K_{eq}) of the probes were estimated based on the intensity of the fluorescent signal obtained in the titration experiments. The calculation method was performed by following the previously reported procedures [51]. The LOD values for **1**-**3** were found to be 64.3, 59.9 and 28.9 nM, respectively. Furthermore, the equilibrium binding constant (K_{eq}) estimated was in the range of 2.4×10^6 – 3.6×10^6 M^{-1} (**Figure S8**). The binding affinity, in terms of dissociation constants K_D, measured by isothermal titration calorimetry (ITC) shown in **Figure S9** was determined in the range of 13.7 – 16.5 μM (**Table 2**). The binding affinity of the ligands determined was comparable and was in micro-molar level.

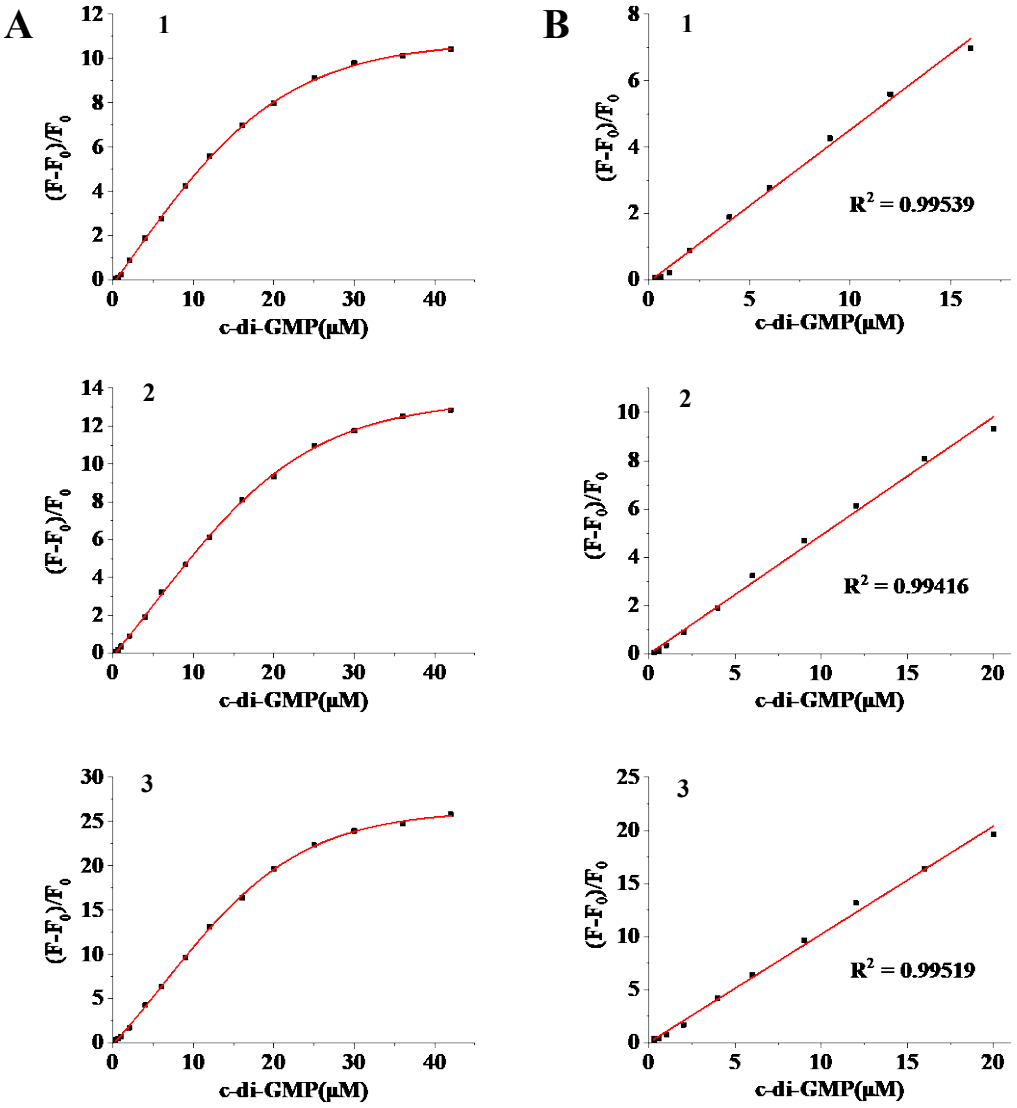

Figure 3. (A) The fluorescence titration of **1-3** (5 μM) with stepwise addition of c-di-GMP (0–42.0 μM). F_0 represents the fluorescence intensity without c-di-GMP and F represents the fluorescence intensity after adding c-di-GMP. (B) Linear relationship curve fitting of the emission intensity of **1-3** (5 μM) with the concentration of c-di-GMP added. The buffer solution used for titrations was Tris-HCl (10 mM, pH 7.5) containing 60 mM KCl.

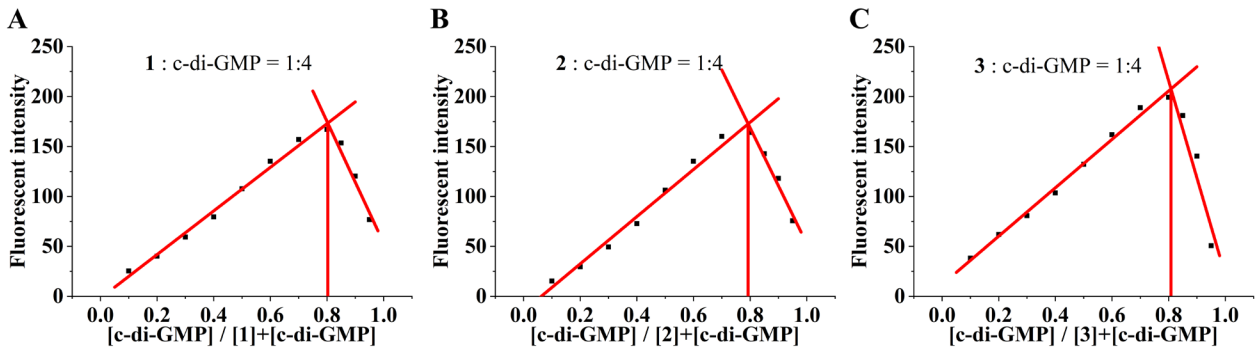

Figure 4. Job plot analysis for the binding stoichiometry of the interaction for the ligand with c-di-GMP in solution. (A) ligand **1**. (B) ligand **2**. (C) ligand **3**. The total concentration of the ligand and c-di-GMP was 20 μM. The buffer used for titration was Tris-HCl (10 mM, pH 7.5) containing 60 mM KCl. λ_{ex}= 442 nm, λ_{em}= 636 nm.

Table 2. The molecular binding property of the fluorescent probes in sensing of c-di-GMP tetramer.

Probe [a]	F/F_0	L_rd (μM) [b]	LOD (nM) [c]	R^2	K_D (μM) [d]
1	11.39	0.285-16.0	64.3	0.99539	16.5
2	13.85	0.285-20.0	59.9	0.99416	13.7
3	26.81	0.285-20.0	28.9	0.99519	15.6

[a] The concentration of probes used was 5.0 μM and the final concentration of c-di-GMP was 42.0 μM. Buffer solution used for assays was Tris-HCl (10 mM, pH 7.5) containing 60 mM KCl.

[b] Linear concentration range for the detection of c-di-GMP.

[c] Limit of detection for c-di-GMP.

[d] Dissociation constant of the probe interacting with c-di-GMP determined with isothermal titration calorimetry at 25 °C.

We speculated that the binding species of c-di-GMP with the probe could be a higher-order tetrameric structure that was found existing in nature and being as an important bacterial secondary messenger that mediates the dimerization of a transcription factor (BldD), which controlled the

progression of multicellular differentiation in sporulating actinomycete bacteria [49]. We then used Job plot to determine the stoichiometric ratio of the *in-situ* formed c-di-GMP-ligand complex. The Job plot results shown in **Figure 4** indicate that the stoichiometric binding ratio of ligands **1**-**3** to c-di-GMP are all 1:4. Therefore, the determined stoichiometric binding ratio may support that the ligand complexed with a higher-order c-di-GMP structure that most likely is a tetramer, which is assembled with four monomeric c-di-GMP molecules (**Figure 1**) to form a guanine (G) quartet-like structure that can be stabilized by cationic ions or small molecules [43, 44]. The structures of G-quartet or G-quadruplex can be imaged selectively for real-time visualization in live cells with fluorescent probes [52-54]. The cellular biofunctions may also be disrupted *via* the molecular interactions [55, 56].

It was reported that the higher-order tetrameric structure of c-di-GMP showed a distinctive and positive circular dichroism (CD) absorption peak at 300-320 nm region [42]. We thus used CD spectroscopy to investigate the interaction of **3** with c-di-GMP and to study if tetrameric structure formed *in-situ* at micromolar concentration condition. From **Figure 5A**, c-di-GMP under the conditions without K^+ ion, the CD absorption was found negative in that range; however, with the addition of 50 mM K^+ ion, the CD absorption in that region was markedly increased to be more positive. The finding is in accord with literature reports that K^+ ion and cationic small molecules can stabilize the tetrameric c-di-GMP structure [42, 43]. For the addition of **3** at 30 μM to the c-di-GMP solution with 50 mM K^+ ion, the CD absorption was also increased remarkably and a positive peak at 307 nm was appeared. Further increasing the concentration of K^+ ion enhances the CD absorption signal at 307 nm, which may indicate the formation of higher order tetrameric c-di-GMP structure. The result obtained is consistent with the 1:4 binding stoichiometry determined with Job plot analysis for **3** interacting with c-di-GMP in solution (**Figure 4**).

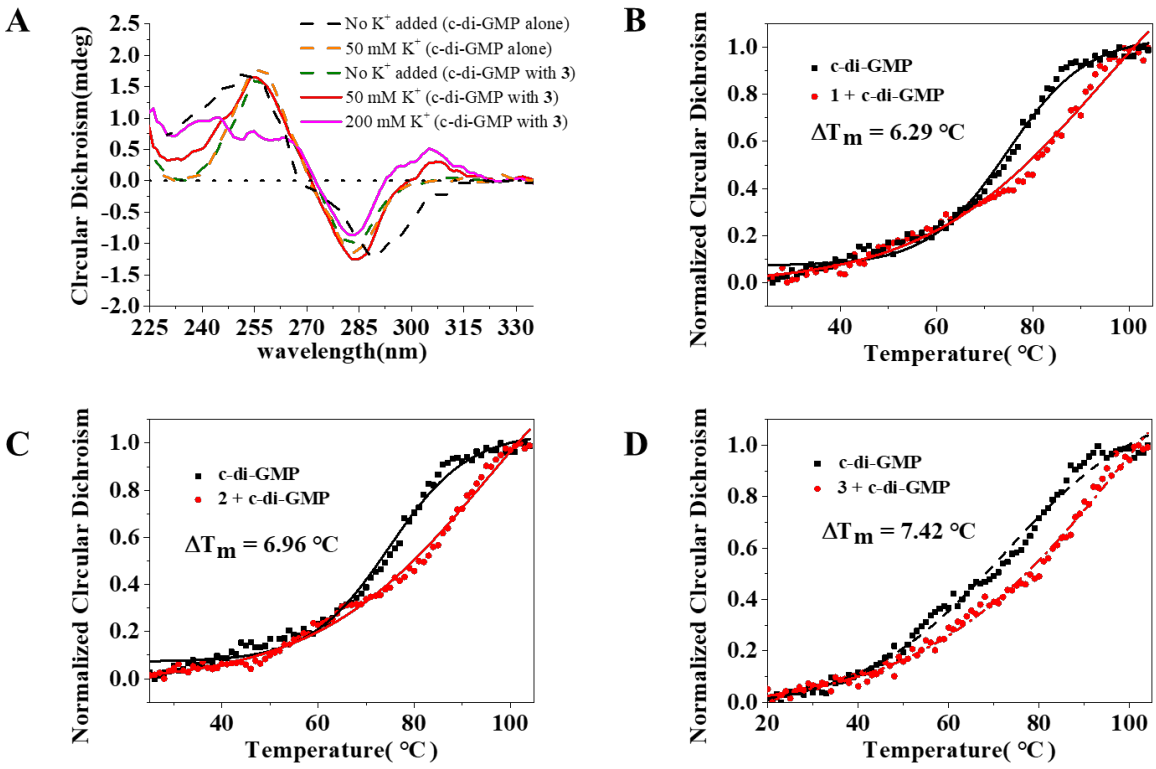

Figure 5. (A) Circular Dichroism of c-di-GMP alone and c-di-GMP-**3** complexes. [c-di-GMP] = 70 μM, [**3**] = 30 μM. Buffer: Tris-HCl (10 mM, pH 7.5) containing KCl at various concentrations. (B)-(D) Melting point change of fluorescent probes after binding with c-di-GMP. [c-di-GMP] = 70 μM, [**3**] = 30 μM. Buffer: Tris-HCl (10 mM, pH 7.5) containing 60 mM KCl.

To investigate the ability of the probe in the stabilization of the higher-order tetrameric c-di-GMP structure upon interaction, melting point assays were conducted. **Figure 5B-D** showed the normalized CD signal profile of c-di-GMP-probe complexes during the melting process. We found that the stabilization ability of these probes was comparable and the ΔT_m obtained was in the range of 6.3-7.4 °C. Nonetheless, **3** showed a slightly better ΔT_m value (7.4 °C) probably due to terminal hydroxyl group of the amino side chain extended at the 2-position of the 1-methylquinolinium scaffold that may be able to provide extra hydrogen bond interaction with the residues of the c-di-

GMP tetramer. The photostability of the probes was also investigated and found that they were highly robust against photo-bleaching over a period of 1 h excited at 442 nm (**Figure S10**).

3.3 Investigation of the interaction of the probe with c-di-GMP using proton NMR spectroscopy and molecular docking study

Our results obtained thus far support that the probe may probably interact with the higher-order tetrameric c-di-GMP structure in solution. To have better understanding on the molecular interaction, we thus investigated the *in-situ* complex of c-di-GMP formed with **3** using 1D proton NMR spectroscopy analysis. As shown in **Figure 6A**, c-di-GMP at 1 mM showed a number of proton signals for the H8 and H1', indicating several oligomeric species formed including the intercalated dimer, tetramer and octamer [33, 42]. It was found that c-di-GMP under the condition with 60 mM K^+ was able to form some higher-order structures including tetramer and octamer; however, the major forms were monomer and dimer. We then introduced **3** at different concentrations to the solution and studied its influence on the proton signals (**Figure 6B**). For the first addition (**3** at 100 μM), the proton signal of the c-di-GMP *anti*-form tetramer (**Ta**) and both *anti*- and *syn*-form octamers (**Os**, **Oa**) disappeared. Interestingly, the signal of *syn*-form tetramer (**Ts**) was retained but the chemical shift was moved to downfield. Further increasing the concentration of **3** (at 200 μM), the proton signal of the c-di-GMP monomer and dimer was reduced markedly and the two originally merged peaks (**M** and **D**) were completely separated. More importantly, the proton signal for *syn*-form tetramer (**Ts**) was significantly increased and further shifted to downfield, and became the major peak of the spectrum. The NMR titration results support that the probe may primarily interact with the *syn*-form tetramer (**Ts**) and then stabilize the **3**-tetramer complex.

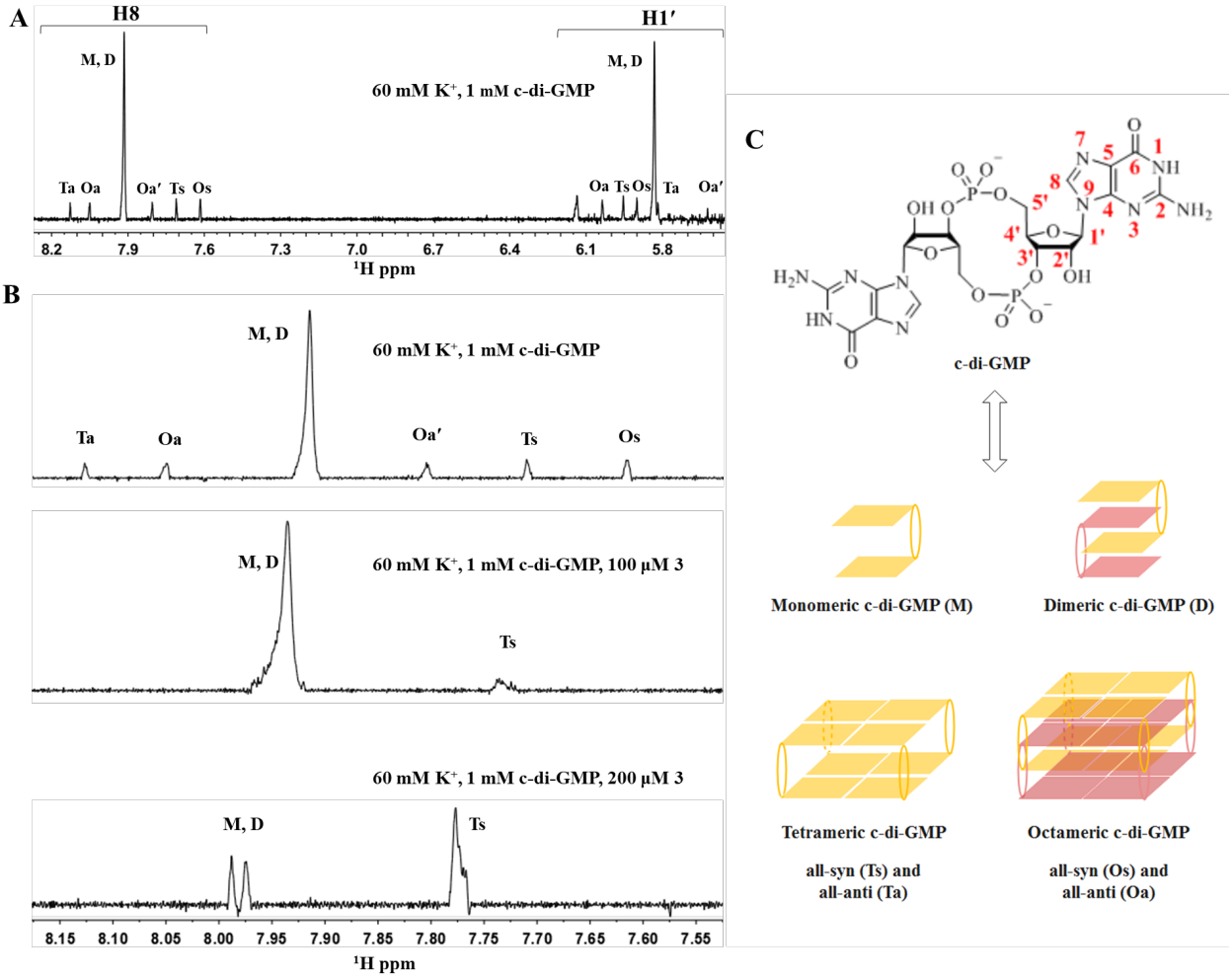

Figure 6. 1D ^{1}H NMR spectra of c-di-GMP under different titration conditions with **3**. (A) H8, and H1′ resonances of 1 mM c-di-GMP. The proton NMR assignments for tetramers (**Ta**, **Ts**) and octamers (**Oa**, **Oa′**, **Os**) were taken from literature [33, 42]. (B) H8 region of the spectrum of 1 mM c-di-GMP in the presence of K^+ ion and **3**. (C) Schematic diagram of the structure of c-di-GMP monomer **M**; dimer **D**; tetramers **Ts**, **Ta**; octamers **Os**, **Oa**.

To obtain more information about the interaction mode of **3** with c-di-GMP tetramer, molecular docking study was performed with the probe and an *X*-ray crystal structure of tetrameric c-di-GMP (PDB ID: 4oay) [49]. The docking result was showed in **Figure 7** and revealed that **3** was in complex with the tetrameric c-di-GMP structure (binding energy = -5.1 kcal/mol). The 1-methylquinolinium scaffold of **3** stacked on the c-di-GMP structure mainly *via* π-π stacking with the guanine residue.

Moreover, the oxygen atom from the hydroxyl group of the probe is forming hydrogen bond interactions with the amide group of the guanine residue of c-di-GMP. These interactions may stabilize the complex. It is supported by its markedly increased melting point (**Figure 5D**, ΔT_m = 7.4 °C) of the adduct. The interaction also restricts the free rotation of the probe and thus leads to intensive red fluorescence signal of the complex upon excited at 442 nm.

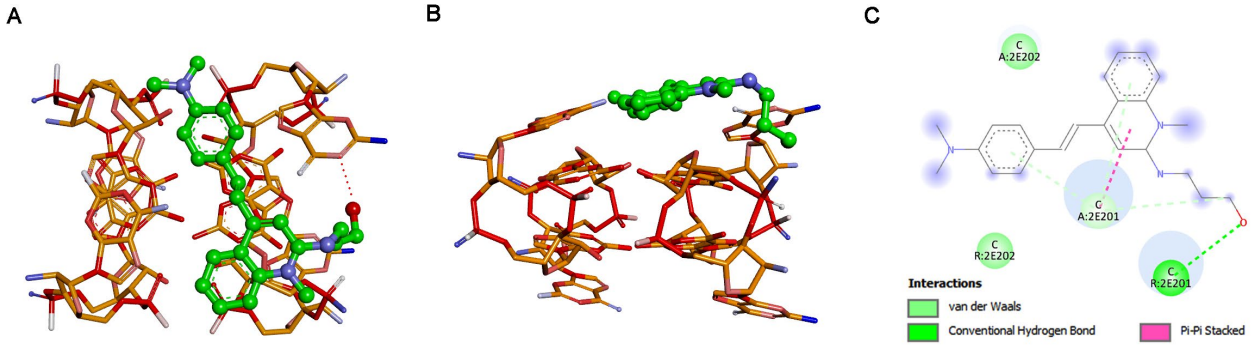

Figure 7. Molecular docking study: (A) top view and (B) side view of **3** in complex with tetrameric c-di-GMP structure from molecular docking study and their interactions. The binding energy of the best docked result = -5.1 kcal/mol. The c-di-GMP tetramer is shown in stick while **3** is shown in green ball and stick. (C) An illustration of the predicted interaction sites of **3** with c-di-GMP tetramer.

3.4 Confocal microscopy imaging of c-di-GMP tetramer in live bacterial cells and monitoring of biofilm formation

Real-time tracking and imaging of c-di-GMP in any form in living bacteria are very significant because c-di-GMP is recognized as one of the most important and widespread second messengers in bacteria [49]. In bacterial cells, potassium ion (K^+) is one of the major intracellular cations. For example, *Staphylococcus aureus* maintains a high intracellular concentration of K^+ ion in the range of 0.5–1.5 M [57]. Since **3** has excellent red fluorescence enhancement upon interaction with c-di-GMP tetramer, we therefore utilize confocal microscopy to study its bioimaging performance in live *Pseudomonas aeruginosa* PAO1 (**Figure 8** A-D) and *Bacillus subtilis* 168 (**Figure 8** E-I). The

bacteria in their division stage were used for imaging study because the bacterial morphology was easy to be observed. The maximum fluorescence intensity for staining PAO1 was achieved in 5 min (**Figure S5B**). From live cell images, the blue area stained by DAPI was the nucleoid region that was located in the middle of the bacteria, while **3** (red fluorescent staining) was mainly located in the cytoplasm. The merged images showed clearly no observable co-localization for **3** and DAPI in both live PAO1 and *Bacillus subtilis* cells. The results may indicate that **3** has excellent selectivity for c-di-GMP. The results demonstrated that **3** was able to induce c-di-GMP to form tetramer and the molecular interaction generated intensive red fluorescence signal both *in vitro* and in live bacterial cells; however, due to the complicated sensing environment in live cells, the possibility of the probe interacting with monomer, dimer and higher-order oligomers cannot be eliminated.

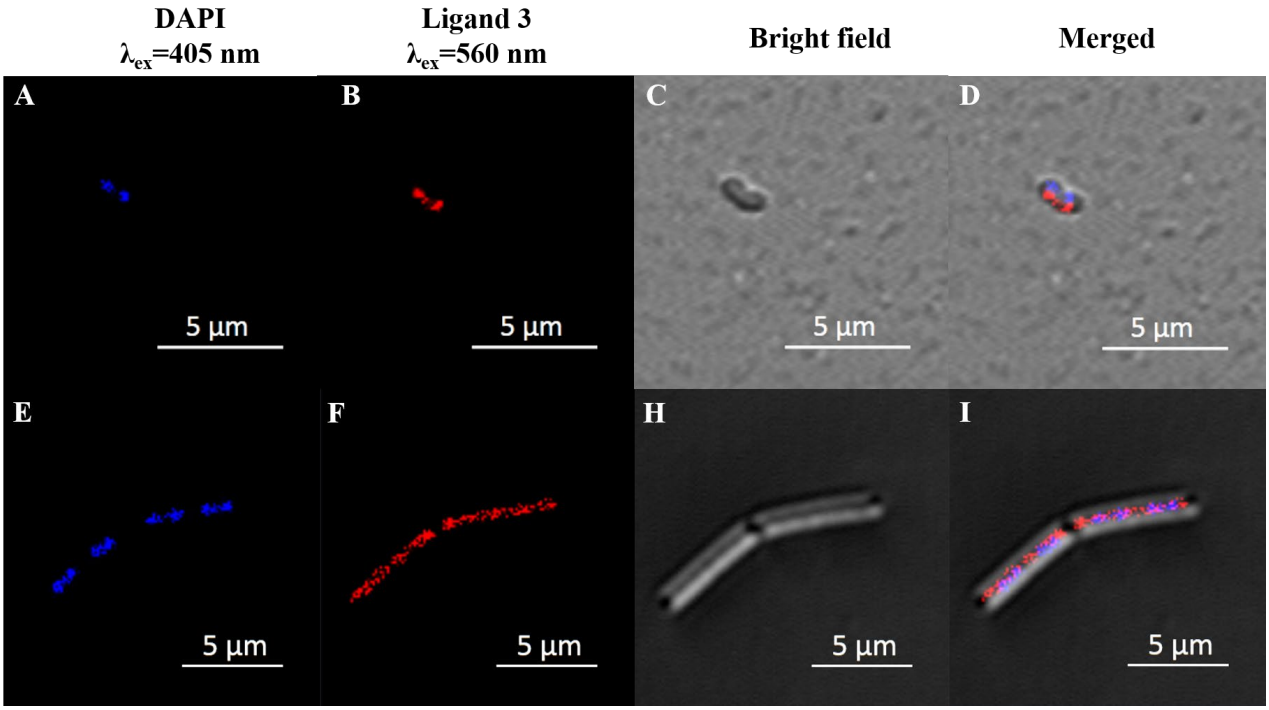

Figure 8. Fluorescent staining of live bacterial cells targeting c-di-GMP in the cell division stage (cells were stained with 10 μM **3** and 1 μM DAPI for 5 min). (A)-(D) in live *Pseudomonas aeruginosa* PAO1; (E)-(I) in live *Bacillus subtilis* 168.

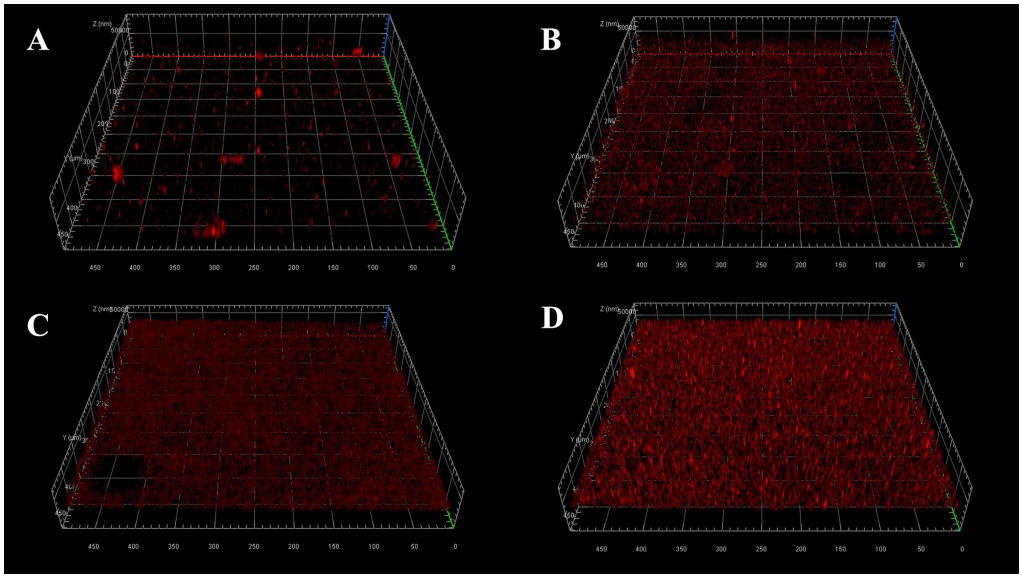

Figure 9. Monitoring of biofilm formation with **3** (10 μM). The 3D images of biofilm of *Pseudomonas aeruginosa* PAO1 grown for (A) 4 h; (B) 6 h; (C) 8 h and (D) 18 h. A video for the visualization of biofilms was attached (Video 1).

Since the probe exhibited excellent sensing performance targeting c-di-GMP, we thus attempted to make use of this unique feature to monitor and visualize the bacterial biofilm formation. Probe **3** was co-incubated with *Pseudomonas aeruginosa* PAO1 and the 3D fluorescence distribution was observed by confocal microscopy when bacteria were grown for 4 h, 6 h, 8 h and 18 h, respectively. The 3D images were shown in **Figure 9**. A video recording the growing process was also given (Video 1). It was clear to observe that, in the early stage of bacterial growth (0-4 h), only weak and scattered red fluorescence was observed in the field of view (**Figure 9A**), indicating that a few biofilms were started to form at these locations. With the gradual growth of bacteria (6 - 8 h), the red fluorescence staining in the field of view was found increased markedly (**Figure 9B** and **C**). After growing for 18 h, the red fluorescence staining spread over the entire field of view and the red fluorescence was very intensive (**Figure 9D**). Therefore, **3** is an excellent and novel fluorescence turn-on biosensor targeting c-di-GMP tetramer. It may have potential applications for monitoring

and visualizing of biofilm formation on both biotic and abiotic surfaces [58]. It is particularly significant to utilize fluorescent sensors such as **3** to track and visualize biofilms that persist on medical device surfaces and on patient's tissues causing persistent infections. Furthermore, the co-staining assays for the biofilm of PAO1-GFP shown in **Figure 10** confirmed that the fluorescence signal of **3** was well co-localized with the green fluorescence emitted from GFP. The live cell imaging results support that **3** is able to track and image biofilm formation in real-time by targeting c-di-GMP in live bacterial cells.

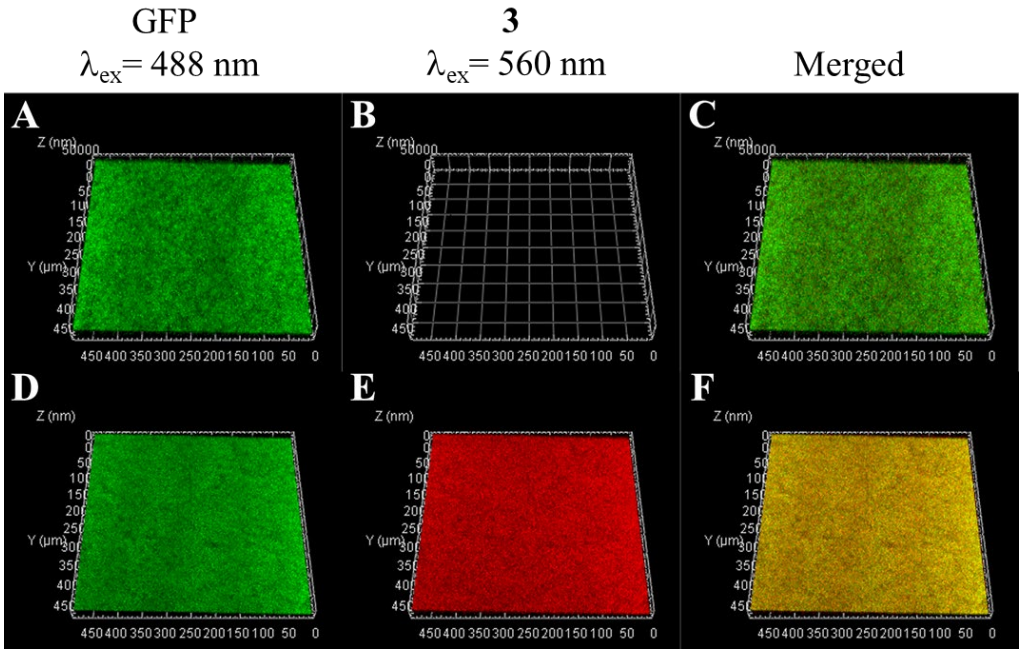

Figure 10. The 3D images of the biofilm of PAO1-GFP grown for 18 h. (A)-(C): Control experiments; GFP-tagged *P. aeruginosa* (PAO1-GFP) biofilm without staining. (D)-(F): The biofilm co-stained with 10 μM ligand **3** for 5 min.

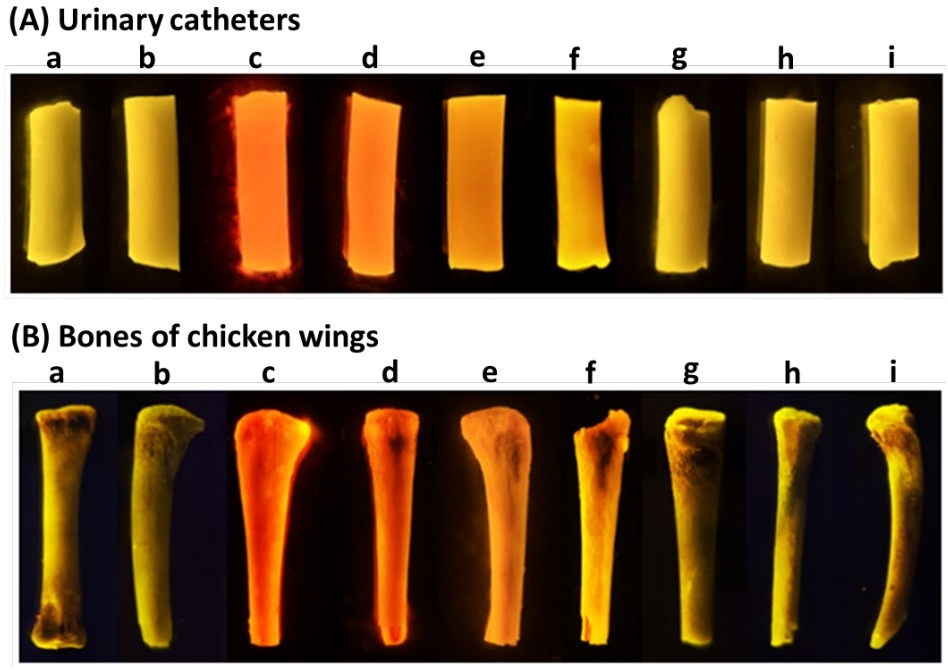

Figure 11. Real-time imaging of biofilms formed on abiotic and biotic surfaces. The red fluorescence signal observed by naked eye under the irradiation with a portable blue LED illuminator (470 nm; 30 W). (A) The urinary catheters and (B) Bones of cooked chicken wings. Experiment conditions for **a-i**: **a**. No treatment; **b**. PAO1 only; **c**. PAO1 + **3** (10 μM); **d**. PAO1 + **3** (10 μM) + 0.05 μg/mL ceftazidime; **e**. PAO1 + **3** (10 μM) + 0.25 μg/mL ceftazidime; **f**. PAO1 + **3** (10 μM) + 0.5 μg/mL ceftazidime; **g**. PAO1 + **3** (10 μM) + 2.0 μg/mL ceftazidime; **h**. PAO1 + 2.0 μg/mL ceftazidime; **i**. 2 μg/mL ceftazidime + **3** (10 μM).

To demonstrate further probe **3** capable of imaging biofilms formed on abiotic and biotic surfaces, naked-eye visualization of PAO1 biofilms grew on the surface of urinary catheters and chicken wing bones under different conditions were studied. The real-time imaging results were shown in **Figure 11**. Under the irradiation with a portable blue LED illuminator at 470 nm, for the experimental conditions: **c**, **d**, **e**, and **f**, the red fluorescent signal can be clearly observed by naked-eye for surfaces of urinary catheters and chicken wing bones with biofilms attached. For condition **c** without treating with ceftazidime (an effective antibiotic inhibiting the growth of biofilms), the

intensity of the red fluorescence enhanced was the strongest. When increasing the concentration of ceftazidime in the assays from 0.05 to 2.0 μg/mL (conditions: **d**, **e**, **f**, and **g**), the enhanced fluorescence was weakened markedly and no fluorescence was observed with 2.0 μg/mL ceftazidime (condition: **g**). Nonetheless, controls showed that no red fluorescent staining signal was observed for the surface with no biofilm attached. These results indicate that with **3** may provide instant, real-time imaging and tracking of biofilms attached on both biotic and abiotic surfaces.

In addition, the cytotoxicity of **3** against two human cell lines (HK-2 and 16HBE) were evaluated. The cell viabilities of **3** at 10 μM were found higher than 75% (**Figure S11**), which indicated that the compound generally exhibited low toxicity toward human kidney and epithelial cells. Therefore, the compound may show potential for practical applications in imaging and monitoring of bacterial biofilms growth on the medical devices and implants [59-61], which have a high risk of causing biofilm-related infections clinically.

Conclusion

In conclusion, a series of red fluorescent probes was demonstrated for rapid sensing and imaging of tetrameric c-di-GMP structure both *in vitro* and in live bacterial cells. A limit of detection (LOD) down to 28.9 nM for the biosensor was achieved. The probe was found highly specific binding to the tetramer of c-di-GMP (a G4-structure) and forming a stable complex. This was supported by the ^{1}H NMR study and competition assays in which a panel of other nucleotides, including GMP, cGMP, deoxy-ribonucleoside triphosphates (dATP, dGTP, dCTP and dTTP) and ribonucleoside triphosphates (rGTP, rATP, rCTP and rUTP), were not able to compete with the c-di-GMP tetramer to interact with **3**. The molecular docking study also suggests that the probe may mainly interact with the tetramer *via* π-π stacking with the guanine residue. Moreover, the molecular interaction

may be further enhanced by the oxygen atom from the hydroxyl group of the probe that forms hydrogen bond with the amide group of the guanine residue of c-di-GMP. Furthermore, the c-di-GMP tetramer upon stained with the probe in live *Pseudomonas aeruginosa* PAO1 and *Bacillus subtilis* 168 could be visualized under a confocal microscope. The real-time monitoring and imaging of bacterial biofilm formation on both biotic and abiotic surfaces (observed by naked-eye) can also be achieved with the probe under the irradiation with a portable blue LED illuminator.

Acknowledgments

The work was substantially supported by the grants from the Research Grants Council of the Hong Kong Special Administrative Region, China (RGC Project No. 15300522), Health and Medical Research Fund (HMRF), Hong Kong SAR (Project No. 19200231), PolyU Startup Fund (P0035712), PolyU SZRI fund (P0039278 and P0039497), National Natural Science Foundation of China (81473082, 22077020 and 32050410289), Natural Science Foundation of Guangdong Province, China (2017A030313078, 2017A030313071, and 2019A1515011799), Department of Education of Guangdong Province, China (2016KCXTD005 and 2017KSYS010), Department of Agriculture and Rural Affairs of Guangdong Province, China (2018LM2175), and Special Funds for the Cultivation of Guangdong College Students' Scientific and Technological Innovation (pdjh2020a0175). In addition, we would like to thank Dr. Xiao Zhou and Dr. Hang Bai from the Analysis and Test Center, Guangdong University of Technology for their assistance in cell imaging experiments.

Data availability

The data supporting the study are also available from the corresponding authors upon reasonable request.

Conflict of interest statement

W.-L.W. submitted a proposal using the results of the present study to the Research Grants Council of the Hong Kong Special Administrative Region, China (RGC Ref. No. 25300523) for competition of research funding.

References

[1] P. Ross, H. Weinhouse, Y. Aloni, D. Michaeli, P. Weinberger-Ohana, R. Mayer, S. Braun, E. de Vroom, G.A. van der Marel, J.H. van Boom, M. Benziman, Regulation of cellulose synthesis in Acetobacter xylinum by cyclic diguanylic acid, Nature 325 (1987) 279-281.

[2] R.R. McCarthy, M.J. Mazon-Moya, J.A. Moscoso, Y. Hao, J.S. Lam, C. Bordi, S. Mostowy, A. Filloux, Cyclic-di-GMP regulates lipopolysaccharide modification and contributes to Pseudomonas aeruginosa immune evasion, Nature microbiology 2 (2017) 1-10.

[3] S. Mudgal, K. Manikandan, A. Mukherjee, A. Krishnan, K.M. Sinha, Cyclic di-AMP: Small molecule with big roles in bacteria, Microbial pathogenesis 161 (2021) 105264.

[4] R. Hengge, Principles of c-di-GMP signalling in bacteria, Nature Reviews Microbiology 7 (2009) 263-273.

[5] U. Romling, M.Y. Galperin, M. Gomelsky, Cyclic di-GMP: the first 25 years of a universal bacterial second messenger, Microbiol Mol Biol Rev 77 (2013) 1-52.

[6] C. Pesavento, R. Hengge, Bacterial nucleotide-based second messengers, Current opinion in microbiology 12 (2009) 170-176.

[7] C.-S. Hee, J. Habazettl, C. Schmutz, T. Schirmer, U. Jenal, S. Grzesiek, Intercepting second-messenger signaling by rationally designed peptides sequestering c-di-GMP, Proceedings of the National Academy of Sciences 117 (2020) 17211-17220.

[8] Y. Fu, Z. Yu, S. Liu, B. Chen, L. Zhu, Z. Li, S.-H. Chou, J. He, c-di-GMP regulates various phenotypes and insecticidal activity of gram-positive Bacillus thuringiensis, Frontiers in microbiology 9 (2018) 45.

[9] C.L. Hall, V.T. Lee, Cyclic-di-GMP regulation of virulence in bacterial pathogens, Wiley Interdisciplinary Reviews: RNA 9 (2018) e1454.

[10] M. Valentini, A. Filloux, Biofilms and cyclic di-GMP (c-di-GMP) signaling: lessons from Pseudomonas aeruginosa and other bacteria, Journal of Biological Chemistry 291 (2016) 12547-12555.

[11] R. Roy, M. Tiwari, G. Donelli, V. Tiwari, Strategies for combating bacterial biofilms: A focus on anti-biofilm agents and their mechanisms of action, Virulence 9 (2018) 522-554.

[12] A. Petchiappan, S.Y. Naik, D. Chatterji, Tracking the homeostasis of second messenger cyclic-di-GMP in bacteria, Biophysical Reviews 12 (2020) 719-730.

[13] M.T. Rybtke, B.R. Borlee, K. Murakami, Y. Irie, M. Hentzer, T.E. Nielsen, M. Givskov, M.R. Parsek, T. Tolker-Nielsen, Fluorescence-based reporter for gauging cyclic di-GMP levels in Pseudomonas aeruginosa, Applied and environmental microbiology 78 (2012) 5060-5069.

[14] C.A. Rodesney, B. Roman, N. Dhamani, B.J. Cooley, P. Katira, A. Touhami, V.D. Gordon, Mechanosensing of shear by Pseudomonas aeruginosa leads to increased levels of the cyclic-

di-GMP signal initiating biofilm development, Proceedings of the National Academy of Sciences 114 (2017) 5906-5911.
[15] H.A. Nair, S. Periasamy, L. Yang, S. Kjelleberg, S.A. Rice, Real time, spatial, and temporal mapping of the distribution of c-di-GMP during biofilm development, Journal of Biological Chemistry 292 (2017) 477-487.
[16] D.O. Serra, R. Hengge, A c-di-GMP-based switch controls local heterogeneity of extracellular matrix synthesis which is crucial for integrity and morphogenesis of Escherichia coli macrocolony biofilms, Journal of molecular biology 431 (2019) 4775-4793.
[17] S. Nakayama, Y. Luo, J. Zhou, T.K. Dayie, H.O. Sintim, Nanomolar fluorescent detection of c-di-GMP using a modular aptamer strategy, Chemical communications 48 (2012) 9059-9061.
[18] C.A. Kellenberger, S.C. Wilson, J. Sales-Lee, M.C. Hammond, RNA-based fluorescent biosensors for live cell imaging of second messengers cyclic di-GMP and cyclic AMP-GMP, Journal of the American Chemical Society 135 (2013) 4906-4909.
[19] X.C. Wang, S.C. Wilson, M.C. Hammond, Next-generation RNA-based fluorescent biosensors enable anaerobic detection of cyclic di-GMP, Nucleic acids research 44 (2016) e139-e139.
[20] J. Yeo, A.B. Dippel, X.C. Wang, M.C. Hammond, In vivo biochemistry: single-cell dynamics of cyclic Di-GMP in Escherichia coli in response to zinc overload, Biochemistry 57 (2018) 108-116.
[21] C.A. Weiss, J.A. Hoberg, K. Liu, B.P. Tu, W.C. Winkler, Single-cell microscopy reveals that levels of cyclic di-GMP vary among Bacillus subtilis subpopulations, Journal of bacteriology 201 (2019) e00247-00219.
[22] H. Zhou, C. Zheng, J. Su, B. Chen, Y. Fu, Y. Xie, Q. Tang, S.-H. Chou, J. He, Characterization of a natural triple-tandem c-di-GMP riboswitch and application of the riboswitch-based dual-fluorescence reporter, Scientific reports 6 (2016) 1-13.
[23] K.-H. Chin, W.-T. Kuo, Y.-J. Yu, Y.-T. Liao, M.-T. Yang, S.-H. Chou, Structural polymorphism of c-di-GMP bound to an EAL domain and in complex with a type II PilZ-domain protein, Acta Crystallographica Section D: Biological Crystallography 68 (2012) 1380-1392.
[24] N.V. Mushnikov, A. Fomicheva, M. Gomelsky, G.R. Bowman, Inducible asymmetric cell division and cell differentiation in a bacterium, Nature chemical biology 15 (2019) 925-931.
[25] M. Christen, H.D. Kulasekara, B. Christen, B.R. Kulasekara, L.R. Hoffman, S.I. Miller, Asymmetrical distribution of the second messenger c-di-GMP upon bacterial cell division, Science 328 (2010) 1295-1297.
[26] B.R. Kulasekara, C. Kamischke, H.D. Kulasekara, M. Christen, P.A. Wiggins, S.I. Miller, c-di-GMP heterogeneity is generated by the chemotaxis machinery to regulate flagellar motility, Elife 2 (2013) e01402.
[27] E. Mills, E. Petersen, B.R. Kulasekara, S.I. Miller, A direct screen for c-di-GMP modulators reveals a Salmonella Typhimurium periplasmic L-arginine–sensing pathway, Science signaling 8 (2015) ra57.
[28] C.L. Ho, K.S.J. Chong, J.A. Oppong, M.L.C. Chuah, S.M. Tan, Z.-X. Liang, Visualizing the perturbation of cellular cyclic di-GMP levels in bacterial cells, Journal of the American Chemical Society 135 (2013) 566-569.
[29] E. Petersen, E. Mills, S.I. Miller, Cyclic-di-GMP regulation promotes survival of a slow-replicating subpopulation of intracellular Salmonella Typhimurium, Proceedings of the National Academy of Sciences 116 (2019) 6335-6340.
[30] K. Paul, V. Nieto, W.C. Carlquist, D.F. Blair, R.M. Harshey, The c-di-GMP binding protein YcgR controls flagellar motor direction and speed to affect chemotaxis by a “backstop brake”

mechanism, Molecular cell 38 (2010) 128-139.
[31] A.B. Dippel, W.A. Anderson, R.S. Evans, S. Deutsch, M.C. Hammond, Chemiluminescent biosensors for detection of second messenger cyclic di-GMP, ACS chemical biology 13 (2018) 1872-1879.
[32] A. Dippel, W. Anderson, J. Park, F. Yildiz, M. Hammond, Ratiometric bioluminescent sensors towards in vivo imaging of bacterial signaling, BioRxiv (2019) 798140.
[33] M. Gentner, M.G. Allan, F. Zaehringer, T. Schirmer, S. Grzesiek, Oligomer formation of the bacterial second messenger c-di-GMP: reaction rates and equilibrium constants indicate a monomeric state at physiological concentrations, Journal of the American Chemical Society 134 (2012) 1019-1029.
[34] C. Chan, R. Paul, D. Samoray, N.C. Amiot, B. Giese, U. Jenal, T. Schirmer, Structural basis of activity and allosteric control of diguanylate cyclase, Proceedings of the National Academy of Sciences 101 (2004) 17084-17089.
[35] T.R. Barends, E. Hartmann, J.J. Griese, T. Beitlich, N.V. Kirienko, D.A. Ryjenkov, J. Reinstein, R.L. Shoeman, M. Gomelsky, I. Schlichting, Structure and mechanism of a bacterial light-regulated cyclic nucleotide phosphodiesterase, Nature 459 (2009) 1015-1018.
[36] G. Minasov, S. Padavattan, L. Shuvalova, J.S. Brunzelle, D.J. Miller, A. Baslé, C. Massa, F.R. Collart, T. Schirmer, W.F. Anderson, Crystal structures of YkuI and its complex with second messenger cyclic di-GMP suggest catalytic mechanism of phosphodiester bond cleavage by EAL domains, Journal of biological chemistry 284 (2009) 13174-13184.
[37] A. Tchigvintsev, X. Xu, A. Singer, C. Chang, G. Brown, M. Proudfoot, H. Cui, R. Flick, W.F. Anderson, A. Joachimiak, Structural insight into the mechanism of c-di-GMP hydrolysis by EAL domain phosphodiesterases, Journal of molecular biology 402 (2010) 524-538.
[38] J. Habazettl, M.G. Allan, U. Jenal, S. Grzesiek, Solution Structure of the PilZ Domain Protein PA4608 Complex with Cyclic di-GMP Identifies Charge Clustering as Molecular Readout, Journal of biological chemistry 286 (2011) 14304-14314.
[39] J. Ko, K.-S. Ryu, H. Kim, J.-S. Shin, J.-O. Lee, C. Cheong, B.-S. Choi, Structure of PP4397 reveals the molecular basis for different c-di-GMP binding modes by Pilz domain proteins, Journal of molecular biology 398 (2010) 97-110.
[40] P.V. Krasteva, J.C. Fong, N.J. Shikuma, S. Beyhan, M.V. Navarro, F.H. Yildiz, H. Sondermann, Vibrio cholerae VpsT regulates matrix production and motility by directly sensing cyclic di-GMP, science 327 (2010) 866-868.
[41] M.V. Navarro, N. De, N. Bae, Q. Wang, H. Sondermann, Structural analysis of the GGDEF-EAL domain-containing c-di-GMP receptor FimX, Structure 17 (2009) 1104-1116.
[42] Z.Y. Zhang, S. Kim, B.L. Gaffney, R.A. Jones, Polymorphism of the signaling molecule c-di-GMP, Journal of the American Chemical Society 128 (2006) 7015-7024.
[43] S. Nakayama, I. Kelsey, J.X. Wang, K. Roelofs, B. Stefane, Y.L. Luo, V.T. Lee, H.O. Sintim, Thiazole Orange-Induced c-di-GMP Quadruplex Formation Facilitates a Simple Fluorescent Detection of This Ubiquitous Biofilm Regulating Molecule, Journal of the American Chemical Society 133 (2011) 4856-4864.
[44] S. Nakayama, I. Kelsey, J.X. Wang, H.O. Sintim, c-di-GMP can form remarkably stable G-quadruplexes at physiological conditions in the presence of some planar intercalators, Chemical Communications 47 (2011) 4766-4768.
[45] I. Kelsey, S. Nakayama, H.O. Sintim, Diamidinium and iminium aromatics as new aggregators of the bacterial signaling molecule, c-di-GMP, Bioorganic & Medicinal Chemistry Letters 22 (2012) 881-885.

[46] T.F. Xuan, J. Liu, Z.Q. Wang, W.M. Chen, J. Lin, Fluorescent Detection of the Ubiquitous Bacterial Messenger 3 ',5 ' Cyclic Diguanylic Acid by Using a Small Aromatic Molecule, Frontiers in Microbiology 10 (2020) 3163.
[47] T.F. Xuan, Z.Q. Wang, J. Liu, H.T. Yu, Q.W. Lin, W.M. Chen, J. Lin, Design and Synthesis of Novel c-di-GMP G-Quadruplex Inducers as Bacterial Biofilm Inhibitors, Journal of Medicinal Chemistry 64 (2021) 11074-11089.
[48] J.-Y. Kim, S. Sahu, Y.-H. Yau, X. Wang, S.G. Shochat, P.H. Nielsen, M.S. Dueholm, D.E. Otzen, J. Lee, M.M.S. Delos Santos, Detection of pathogenic biofilms with bacterial amyloid targeting fluorescent probe, CDy11, Journal of the American Chemical Society 138 (2016) 402-407.
[49] N. Tschowri, M.A. Schumacher, S. Schlimpert, N. babu Chinnam, K.C. Findlay, R.G. Brennan, M.J. Buttner, Tetrameric c-di-GMP mediates effective transcription factor dimerization to control Streptomyces development, Cell 158 (2014) 1136-1147.
[50] X.H. Huang, M.T. She, Y.H. Zhang, Y.F. Liu, D.X. Zhong, Y.H. Zhang, J.X. Zheng, N. Sun, W.L. Wong, Y.J. Lu, Novel quinoline-based derivatives as the PqsR inhibitor against Pseudomonas aeruginosa PAO1, Journal of Applied Microbiology 133 (2022) 1-15.
[51] N. Sun, C. Wang, M.-H. Xu, Y.-J. Lu, Y.-Y. Zheng, Y. Yan, X.-L. Guo, J. Hou, K. Zhang, L.G. Luyt, The interaction of a structural flexible small molecule with nucleic acid structures: Investigation of the origin of fluorescence signal discrimination in sensing and the utilization in live cell imaging, Sensors and Actuators B: Chemical 250 (2017) 543-551.
[52] M. Di Antonio, A. Ponjavic, A. Radzevičius, R.T. Ranasinghe, M. Catalano, X. Zhang, J. Shen, L.-M. Needham, S.F. Lee, D. Klenerman, Single-molecule visualization of DNA G-quadruplex formation in live cells, Nature chemistry 12 (2020) 832-837.
[53] P.A. Summers, B.W. Lewis, J. Gonzalez-Garcia, R.M. Porreca, A.H. Lim, P. Cadinu, N. Martin-Pintado, D.J. Mann, J.B. Edel, J.B. Vannier, Visualising G-quadruplex DNA dynamics in live cells by fluorescence lifetime imaging microscopy, Nature communications 12 (2021) 1-11.
[54] M.-T. She, J.-W. Yang, B.-X. Zheng, W. Long, X.-H. Huang, J.-R. Luo, Z.-X. Chen, A.-L. Liu, D.-P. Cai, W.-L. Wong, Design mitochondria-specific fluorescent turn-on probes targeting G-quadruplexes for live cell imaging and mitophagy monitoring study, Chemical Engineering Journal (2022) 136947.
[55] W. Long, B.-X. Zheng, X.-H. Huang, M.-T. She, A.-L. Liu, K. Zhang, W.-L. Wong, Y.-J. Lu, Molecular recognition and imaging of human telomeric G-quadruplex DNA in live cells: a systematic advancement of thiazole orange scaffold to enhance binding specificity and inhibition of gene expression, Journal of Medicinal Chemistry 64 (2021) 2125-2138.
[56] W. Long, B.-X. Zheng, Y. Li, X.-H. Huang, D.-M. Lin, C.-C. Chen, J.-Q. Hou, T.-M. Ou, W.-L. Wong, K. Zhang, Rational design of small-molecules to recognize G-quadruplexes of c-MYC promoter and telomere and the evaluation of their in vivo antitumor activity against breast cancer, Nucleic acids research 50 (2022) 1829-1848.
[57] A. Gründling, Potassium uptake systems in Staphylococcus aureus: new stories about ancient systems, MBio 4 (2013) e00784-00713.
[58] V.O. Silva, L.O. Soares, A. Silva Júnior, H.C. Mantovani, Y.-F. Chang, M.A.S. Moreira, Biofilm formation on biotic and abiotic surfaces in the presence of antimicrobials by Escherichia coli isolates from cases of bovine mastitis, Applied and environmental microbiology 80 (2014) 6136-6145.
[59] J. Fang, Y. Wan, Y. Sun, X. Sun, M. Qi, S. Cheng, C. Li, Y. Zhou, L. Xu, B. Dong, Near-infrared-activated nanohybrid coating with black phosphorus/zinc oxide for efficient biofilm eradication against implant-associated infections, Chemical Engineering Journal 435 (2022) 134935.

[60] Z. Ma, J. Li, Y. Bai, Y. Zhang, H. Sun, X. Zhang, A bacterial infection-microenvironment activated nanoplatform based on spiropyran-conjugated glycoclusters for imaging and eliminating of the biofilm, Chemical Engineering Journal 399 (2020) 125787.
[61] J. Torra, T. Sawazaki, P. Bondia, S. Nonell, M. Kanai, Y. Sohma, C. Flors, Activatable Iodinated BODIPYs for Selective Imaging and Photodynamic Disruption of Amyloid Structures in Pathogenic Bacterial Biofilms, Sensors and Actuators B: Chemical (2022) 132475.